Supramolecular Polymerization as a Tool to Reveal the Magnetic Transition Dipole Moment of Heptazines

Xu, Fan; Su, Hao; van der Tol, Joost J.B.; Jansen, Stef A.H.; Fu, Youxin; Lavarda, Giulia; Vantomme, Ghislaine; Meskers, Stefan; Meijer, E. W.

Published in:
Journal of the American Chemical Society

DOI:
10.1021/jacs.4c02174

JACS
JOURNAL OF THE AMERICAN CHEMICAL SOCIETY
pubs.acs.org/JACS
Article

Supramolecular Polymerization as a Tool to Reveal the Magnetic Transition Dipole Moment of Heptazines

Fan Xu, Hao Su, Joost J. B. van der Tol, Stef A. H. Jansen, Youxin Fu, Giulia Lavarda, Ghislaine Vantomme, Stefan Meskers,* and E. W. Meijer*

Cite This: J. Am. Chem. Soc. 2024, 146, 15843−15849

ABSTRACT: Heptazine derivatives have attracted significant interest due to their small S_1-T_1 gap, which contributes to their unique electronic and optical properties. However, the nature of the lowest excited state remains ambiguous. In the present study, we characterize the lowest optical transition of heptazine by its magnetic transition dipole moment. To measure the magnetic transition dipole moment, the flat heptazine must be chiroptically active, which is difficult to achieve for single heptazine molecules. Therefore, we used supramolecular polymerization as an approach to make homochiral stacks of heptazine derivatives. Upon formation of the supramolecular polymers, the preferred helical stacking of heptazine introduces circular polarization of absorption and fluorescence. The magnetic transition dipole moments for the $S_1 \leftarrow S_0$ and $S_1 \rightarrow S_0$ are determined to be 0.35 and 0.36 Bohr magneton, respectively. These high values of magnetic transition dipole moments support the intramolecular charge transfer nature of the lowest excited state from nitrogen to carbon in heptazine and further confirm the degeneracy of S_1 and T_1.

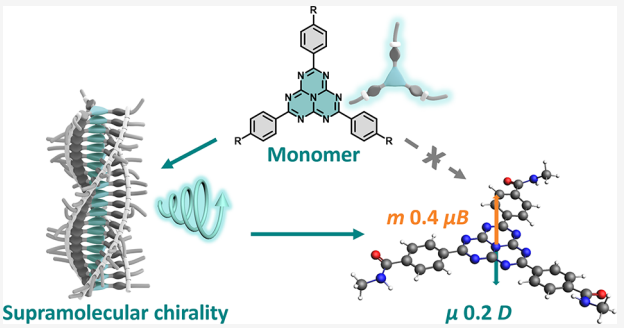

INTRODUCTION

In organic molecular materials, the mean free path of an electron is usually severely limited, and its angular momentum is heavily quenched.[1] Quantum Hall effects, topologically protected conduction states, and other quantum conduction phenomena are practically impossible to realize with organics. The limited size of the molecules, strong coupling with vibrations, and an abundance of crystal defects are to blame. To improve electron delocalization, there is a global effort to design and synthesize molecules with monodisperse mass distribution and extended conjugation.[2−7]

Among extended conjugated carbon nitrides, heptazine has garnered significant attention in recent years owing to its unique electronic and optical properties, for instance, thermally activated delayed fluorescence (TADF).[8,9] By designing specific structures, inverted singlet and triplet excited states are proposed, which breaks Hund's rule.[10,11] Furthermore, heptazine derivatives find applications in various fields, for instance, photocatalysis of water splitting.[8,12−15] These unique electronic and optical properties are closely related to its lowest excited state.[8−14] However, the precise nature of the lowest excited state of heptazine remains unclear.

The magnetic transition dipole is among the first-order terms in a series expansion of the interaction of the molecule underdoing the transition with the electromagnetic field.[16] As a result, it reflects the nonlocal response of the molecules that is expected when the coherence length of the wavefunction is no longer negligible compared to the wavelength of light. The magnetic transition dipole moment ($\boldsymbol{m}$) describes the circular component of the change transfer, indicating the rotation of electrons during the transition; thus, is crucial for unveiling the nature of the lowest excited state.[17] In a truly breathtaking development over the last few years, improvements in synthesis have resulted in molecules with chromophoric centers containing sp^2 hybridized atoms with high $\boldsymbol{m}$.[18−31] These largely conjugated chromophores are intrinsically chiral and are the result of the impressive synthesis and separation of enantiomers. The magnetic transition dipole moment of the enantiomers of chiral molecules can be quantitatively determined from circular dichroism spectroscopy. To date, the determination of the magnetic transition dipole moments of molecules with flat π systems remains challenging, especially for heptazine, which presents a synthetic challenge when attempting to generate chiral variants.

Supramolecular chirality, which refers to the nonsymmetric arrangement of molecules within a noncovalent system,[32,33] emerges as one of the most promising approaches for

Received: February 12, 2024
Revised: May 15, 2024
Accepted: May 16, 2024
Published: May 30, 2024

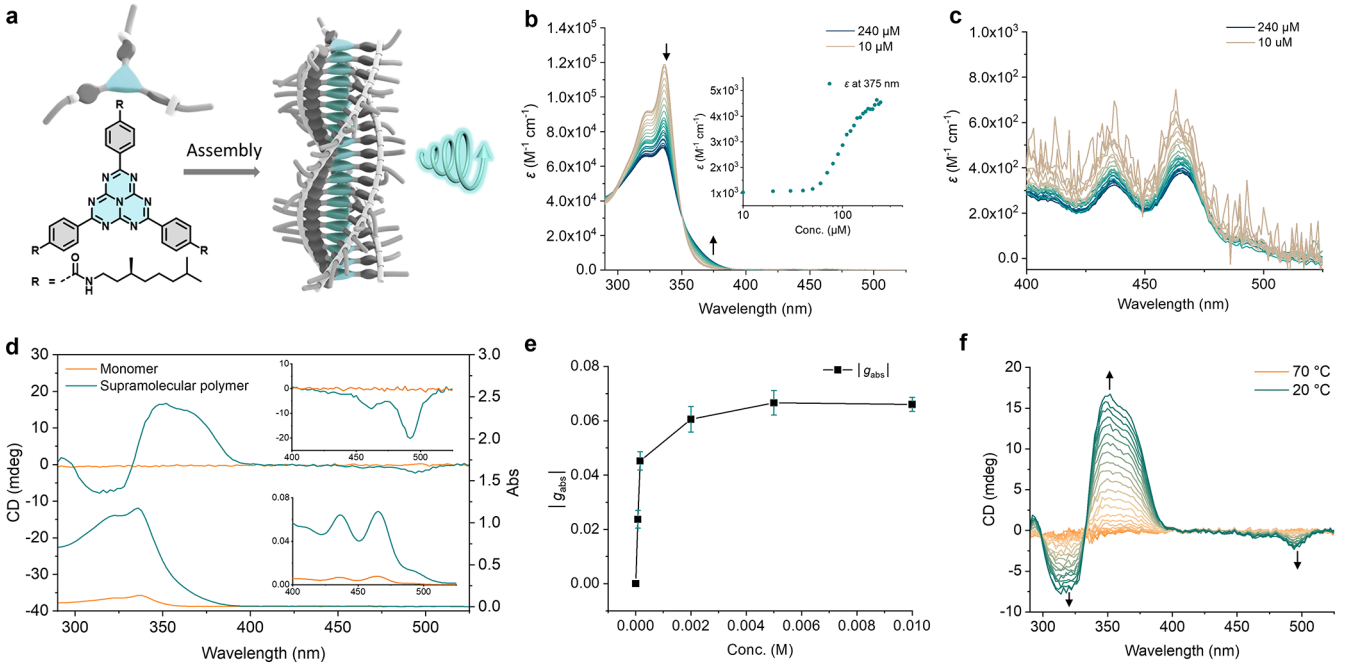

Figure 1. (a) Molecular structure of *S*-**H** and cartoon of a supramolecular polymer of *S*-**H** with circularly polarized luminescence (CPL) (b) Concentration-dependent UV−vis absorption spectra of *S*-**H** (10−240 μM) in toluene, inset: ε at 375 nm of *S*-**H** in toluene at different concentrations, and (c) enlarged spectra between 400 and 525 nm. (d) CD and UV−vis absorption of toluene solution of *S*-**H** in the 1 mm cuvettes at 10 and 160 μM, separately. Inset: CD and UV−vis absorption spectra at the region of 400−525 nm. (To increase the resolution of spectra at the 400−525 nm region, the samples were measured in a 1 cm cuvette). (e) Values of dissymmetry factor of absorption ($|g_{abs}|$) of *S*-**H** in toluene at different concentrations. (f) CD spectra of a toluene solution of *S*-**H** (160 μM) upon cooling with a rate of −2 K min^{-1}.

chiroptoelectronic[34] and spintronics.[35−38] Supramolecular polymers, as one-dimensionally ordered assemblies,[39,40] are one of the best systems for introducing supramolecular chirality.[41−43] They are formed by noncovalent bonding and therefore have significant advantages in terms of dynamics and pathway complexity.[44−50] Their high degree of tunability and versatility provides a valuable complement to traditional covalent polymers and contributes to the creation of adaptive systems and innovative materials.[51−56]

In the present study, we show that supramolecular polymerization can induce a high circular polarization in the optical transition between the ground and the lowest excited singlet state and thus reveal the spatial coherence of the electronic states of molecules. The achiral heptazine core was substituted with chiral alkyl chains, which offer a chiral bias to the helical stacking of heptazine (*S*-**H**) (Figure 1a). The resulting supramolecular polymer exhibits circularly polarized absorption and fluorescence with high dissymmetric factors. The dissymmetric factor and quantum yield of the solution can be controlled by altering the ratio of the solvent mixture. Notably, the resulting high degree of circular polarization in the optical transition between the ground and lowest excited singlet state offers a method to characterize the magnetic transition dipole moment through supramolecular polymerization.

RESULTS AND DISCUSSIONS

The synthesis of *S*-**H** is detailed in the Supporting Information. The assembly behavior of *S*-**H** was studied in toluene by using circular dichroism (CD), UV−vis absorption, ^{1}H NMR, and FT-IR spectroscopy. The absorption spectrum of monomeric dissolved heptazine shows a strong $S_n \leftarrow S_0$ absorption band at 300−375 nm and a very weak $S_1 \leftarrow S_0$ absorption band at 420−515 nm with molar extinction coefficients (ε) of 1.2 × 10^5 and 5 × 10^2 M^{-1} cm^{-1}, respectively, which is comparable with other heptazine derivatives (Figure 1b,c).[8] Concentration-dependent UV−vis spectroscopy measurements in toluene revealed a broadening of the absorption band of $S_n \leftarrow S_0$ with a clear isosbestic point at 351 nm (Figure 1b) due to aggregation, while the shape of the band of $S_1 \leftarrow S_0$ remained consistent (Figure 1c). The critical aggregation concentration (CAC) of approximately 50 μM was determined based on the sharp transition observed in the curve of absorption as a function of concentration (Figure 1b). The formation of one-dimensional aggregates was confirmed by the atomic force microscopy (AFM) studies, in which the diameter of fibers is around 1.2 nm (Figure S1). This diameter closely corresponds to the distance between the center N atom in the heptazine core and the terminal C atom of the alkyl chain in the molecule.

Above the CAC, toluene solutions of *S*-**H** exhibit CD signals at both bands (Figure 1d), suggesting the formation of chiral supramolecular polymers. Changes in the CD signal and UV−vis absorption spectra can be reversibly controlled by heating and cooling (Figures 1f and S2). Plotting the CD signal at 360 nm against different temperatures results in a nonsigmoidal curve with a sharp transition at T_e (Figure S3). To analyze the cooling curves of *S*-**H** at different concentrations, we employed a thermodynamic mass-balance model (details in SI). The fitting results revealed that the supramolecular polymerization of *S*-**H** follows a cooperative mechanism, characterized by an elongation enthalpy ΔH_e of −49.2 kJ mol^{-1}, an entropy ΔS of −84.0 J mol^{-1} K^{-1}, and a nucleation penalty (NP) of 10.2 kJ mol^{-1} (Table S1). We further measured the FT-IR spectra of *S*-**H** in toluene, which indicated the presence of hydrogen-bonded species in the solution, as evidenced by the N−H

https://doi.org/10.1021/jacs.4c02174
J. Am. Chem. Soc. 2024, 146, 15843−15849

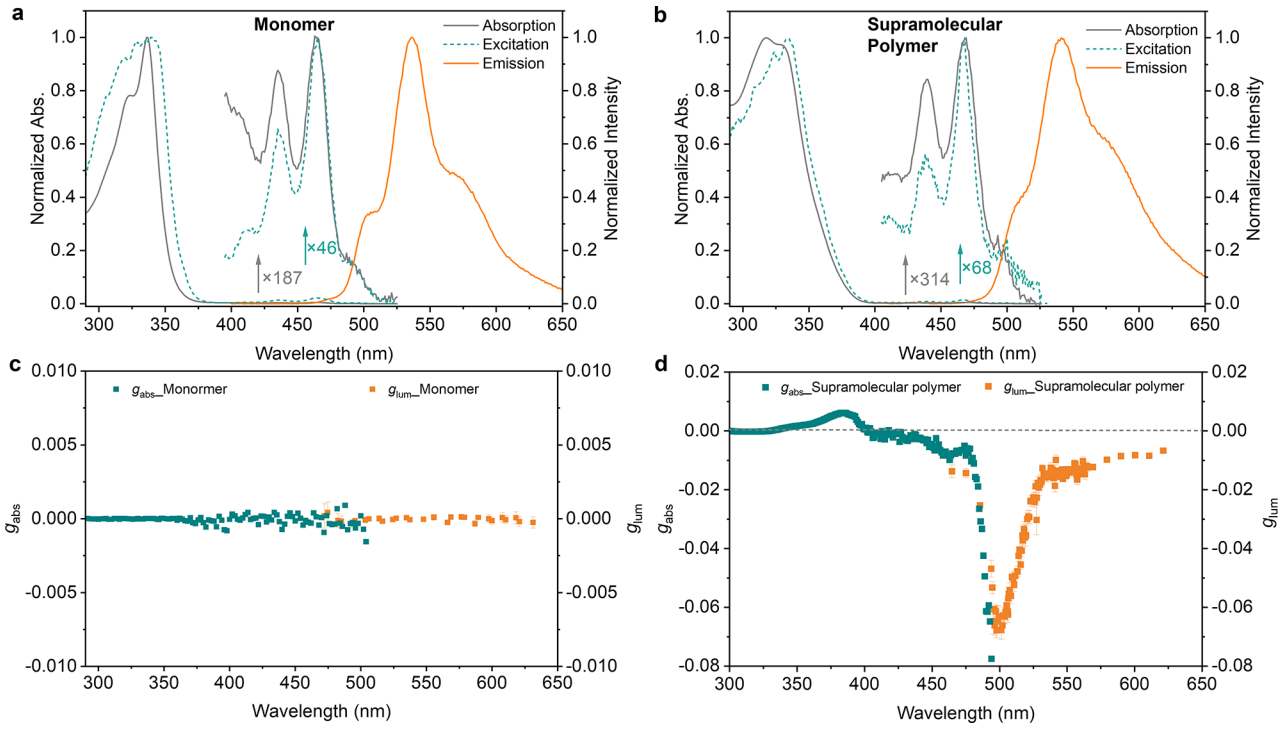

Figure 2. Normalized absorption (gray curve), excitation (green curve), and emission spectra (orange curve) of (a) *S*-**H** monomer (10 μM) in deaerated toluene and (b) supramolecular polymer of *S*-**H** (10 μM) in deaerated toluene/MCH (1/3). g_{abs} and g_{lum} wavelength curves of the (c) *S*-H monomer in toluene and (d) the supramolecular polymer of *S*-**H** in deaerated toluene/MCH (1/3).

stretching vibration at 3257 cm^{-1} and the C=O stretching vibration at 1625 cm^{-1} (Figure S4). Temperature-dependent ^{1}H NMR spectra revealed the upfield shifts of aromatic protons (H^a and H^b) upon cooling, suggesting the occurrence of $\pi-\pi$ stacking among these phenyl groups (Figure S5). Therefore, the heptazine monomers are stacked on top of each other through $\pi-\pi$ stacking and hydrogen bonding to form homochiral supramolecular polymers, following a cooperative mechanism.

When fully aggregated, the dissymmetry factor of the S_0 to S_1 transition (g_{abs}) is −0.067 (Figure 1e), which is much larger than that of the S_0 to S_n transition (g_{abs} = 0.001). Usually, the pure magnetic dipole transitions in the optical frequency range are extremely weak in intensity. Then the associated magnetic transition dipole moment is difficult to determine because extremely small perturbations of the molecular structure (e.g., molecular vibrations) can lead to the mixture of an excited state with an electronic dipole-allowed transition. As a result of this mixing of excited states, the original transition probability, due to the magnetic dipole, can easily be overwhelmed by the admixed electronic dipole strength. However, the significant g_{abs} of *S*-**H** suggests a magnetically allowed transition between S_1 and S_0, offering the possibility to determine the magnetic transition dipole moments.

For determining the magnetic transition dipole moment, we assume D_3 symmetry for the heptazine molecule in the helical aggregate and the lowest excited singlet state of the $\pi-\pi^*$ nature. The lowest $\pi-\pi^*$ state must then have A_2 symmetry in order to be connected to the ground state (S_0) via a magnetic dipole-allowed transition. A_2 symmetry for the lowest excited singlet state is consistent with recent quantum chemical studies.[57] The transition between the S_0 and $S_1(A_2)$ excited states is also electric dipole allowed. Both $\boldsymbol{m}$ and $\boldsymbol{\mu}$ are parallel to the 3-fold symmetry axis and thus the angle between $\boldsymbol{m}$ and $\boldsymbol{\mu}$ can be taken zero. Lastly, when evaluating the magnitude of the component of $\boldsymbol{\mu}$ parallel to the 3-fold axis, contributions to the total electric dipole in a direction perpendicular to the axis induced via vibronic mixing should be eliminated. This is possible because these in-plane components only contribute to the higher vibronic transitions and a procedure to eliminate these contributions is known.[58]

Therefore, we calculated $m_{1\leftarrow 0,z}$ through the following functions:[16]

$$g_{abs} = \frac{2(\varepsilon_L - \varepsilon_R)}{\varepsilon_L + \varepsilon_R} = \frac{4cIm(\vec{m}_{1\leftarrow 0}\cdot\vec{\mu}_{1\leftarrow 0})}{|\vec{m}_{1\leftarrow 0}|^2 + c^2|\vec{\mu}_{1\leftarrow 0}|^2} \quad (1)$$

Here $\Delta\varepsilon = \varepsilon_L - \varepsilon_R$ denotes the circular differential molar decadic extinction coefficient, c is the speed of light, $\vec{m}_{1\leftarrow 0}$ and $\vec{\mu}_{1\leftarrow 0}$ are the magnetic and electronic transition dipole moments for the transition from the singlet ground state 0 to the lowest excited singlet state 1. The sign "*Im*" indicates that the imaginary component should be taken. From S_0 to S_1, the electronic dipole moment $\mu_{1\leftarrow 0,z}$ was determined to be 0.18 D, and the magnetic transition dipole moment $m_{1\leftarrow 0,z}$ was determined as 0.35 Bohr magneton (see details in SI).

For the fluorescence associated with the reverse transition from S_1 to S_0, we studied the circular polarization, the decay after pulsed excitation, and the quantum yield. The emission and excitation spectra of *S*-**H** were measured in deaerated toluene. Monomerically dissolved *S*-**H** (10 μM) displayed two excitation bands at 420−515 and 300−375 nm (Figure 2a). Upon excitation, *S*-**H** emitted green light, with a maximum at 537 nm in the emission spectra (Figure 2a). Monomeric dissolved *S*-**H** did not exhibit circular dichroism (CD) or circularly polarized luminescence (CPL) due to its inherent symmetry of the heptazine core and lack of absorption in the UV−vis region of the chiral alkyl chains. Consequently, both

https://doi.org/10.1021/jacs.4c02174
J. Am. Chem. Soc. 2024, 146, 15843−15849

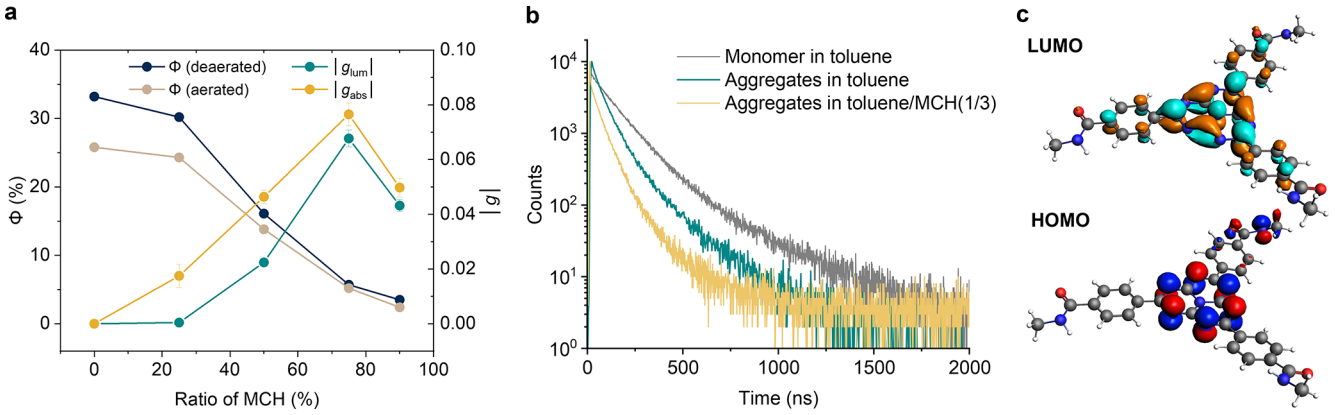

Figure 3. (a) Quantum yield (Φ) and dissymmetric factors ($|g_{lum}|$) of *S*-**H** (10 μM) in the toluene/MCH with different solvent ratios. (b) Photoluminescence traces of *S*-**H** monomer (10 μM) in deaerated toluene and supramolecular polymer (10 mM) in deaerated toluene and (10 μM) in deaerated toluene/MCH (1/3). (c) Distribution of electron density in HOMO and LUMO of *S*-**H** calculated at the hybrid-B3LYP level.

values of g_{abs} and g_{lum} were found to be zero (Figure 2c). In toluene, a high concentration of *S*-**H** is required to obtain a high degree of aggregation. This high concentration of 5−10 mM hindered accurate CPL measurements due to self-absorption and nonpolarized emission contributed from monomers (Figure S6).

To increase the degree of polymerization at lower concentrations, we introduce MCH as a cosolvent. In the mixture of toluene and MCH, UV absorption and CD intensity of *S*-**H** (10 μM) at 360 nm exhibit an increasing trend until MCH exceeded 60% (v%) and then leveled off until MCH exceeded 80% (Figure S8), which suggests that **S-H** was fully aggregated in solvent mixtures containing 60%−80% of MCH. Therefore, we used solvent mixtures containing 75% of MCH (toluene/MCH = 1/3) for the following study. The emission spectrum shows a band centered at 537 nm, the same band as that of the monomer (Figure 2b). Unlike the *S*-**H** monomer, the supramolecular polymer exhibits intense CPL emission (Figure S7). The maximum values of g_{abs} and g_{lum} were determined to be −0.078 and −0.068, respectively (Figure 2d). Interestingly, we found that the g_{lum} of *S*-**H** increased with the ratio of toluene/MCH until 1/3, after which the g_{lum} decreased slightly, while the quantum yield (Φ) decreased from 33% to 4% as the MCH ratio increased (Figure 3a). These alterations in photophysics may be attributed to the degree of supramolecular polymerization (Figure S10). Time-correlated single-photon counting studies revealed a multiexponential photoluminescence decay with two distinct emission lifetimes: 54 and 162 ns of supramolecular polymer in the deaerated toluene/MCH with a ratio of 1/3. After obtaining the data, we calculated $m_{1\to 0,z}$ through the following functions:

$$g_{lum} = \frac{2(I_L - I_R)}{I_L + I_R} = \frac{4cIm(\vec{m}_{1\to 0}\cdot\vec{\mu}_{1\to 0})}{|\vec{m}_{1\to 0}|^2 + c^2|\vec{\mu}_{1\to 0}|^2} \quad (2)$$

Here, $\vec{m}_{1\to 0}$ and $\vec{\mu}_{1\to 0}$ correspond to transition dipole moments for the emissive transition from the lowest excited singlet state back to the ground state. The electronic dipole moment $\mu_{1\to 0,z}$ was determined to be 0.20 D from the fluorescence decay curve and quantum yield via the Strickler−Berg equation (details in SI). Then, the magnetic transition dipole moment $m_{1\to 0,z}$ was determined as 0.36 Bohr magneton, which is close to 0.35 Bohr magneton of $m_{1\leftarrow 0,z}$. These values are also consistent with the result of 0.4 Bohr magneton from quantum chemical calculation of the magnetic transition dipole moment of the heptazine moiety ($C_6H_3N_7$ 1,3,4,6,7,9,9*b*-heptaazaphenalene) with D_{3h} symmetry (see details in SI). These results confirm that the transition between the lowest excited states and the ground state is electronically forbidden but magnetically allowed.

Multiexponential photoluminescence decay was also observed for the monomer of *S*-**H** in deaerated toluene with two emission lifetimes of 122 and 351 ns (Figure S13). In the presence of oxygen, the lifetimes of the *S*-**H** monomers slightly decrease to 104 and 237 ns, respectively (Figure S13). The emission quantum yield (Φ) decreased from 33% in deaerated toluene to 25% in aerated toluene due to the quenching of triplet excited states by oxygen (Figure 3a). The emission spectrum of *S*-**H** remains the same in the presence of oxygen (Figure S12). The small influence of the oxygenation of the sample on the decay of the fluorescence and Φ suggests that the TADF slightly contributes to the emission. Temperature-dependent photoluminescence decay revealed a slight increase of τ upon cooling, suggesting that nonradiative decay is suppressed at low temperatures (Figure S14). In deaerated toluene, the emission lifetimes of supramolecular polymers of *S*-**H** were determined to be 62 and 209 ns, whereas in the deaerated toluene/MCH (1/3), the lifetimes were found to be 54 and 162 ns (Figure 3b). Both of them are shorter than the lifetimes of monomers. The reduced lifetime and Φ of supramolecular polymers indicate faster nonradiative decay in the aggregates. In the presence of oxygen, the lifetime and Φ of supramolecular polymers slightly decrease (Figures S15 and S16), which is consistent with the behavior of monomers and suggests the limited contribution from TADF.

To gain further insights into the photophysics of *S*-**H**, its electronic structure was calculated using time-dependent density functional theory (TDDFT) with the three-parameter Becke−Lee−Yang−Parr hybrid density functional (hybrid-B3LYP). The highest occupied molecular orbital (HOMO) was found exclusively located on the peripheral nitrogen atoms of the heptazine core, with some on the benzoic amide substituents (Figure 3c). Conversely, the lowest unoccupied molecular orbital (LUMO) is primarily distributed on the carbon atoms and the central nitrogen atom of the core. This negligible overlap between the HOMO and LUMO indicates an intramolecular charge transfer nature of the lowest excited state from nitrogen to carbon, which led to a small electronic transition dipole moment but a large magnetic transition

https://doi.org/10.1021/jacs.4c02174
J. Am. Chem. Soc. 2024, 146, 15843−15849

dipole moment between the S_1 and S_0 states. The small electronic transition dipole moment was consistent with the low molar extinction coefficient observed in the UV−vis absorption spectra for the band centered at 465 nm. At the same time, the significant difference in charge distribution on carbon and nitrogen atoms results in a very low exchange energy and an extremely narrow energy gap between the S_1 and T_1 states.

CONCLUSION

Incorporating the planar heptazine chromophore into a homochiral supramolecular polymer results in a high degree of circular polarization in the optical transition between the ground and the lowest excited singlet state. From the circular polarization, the magnetic transition dipole moment for this forbidden transition can be determined and is found to be a 0.4 Bohr magneton. The high value of the magnetic transition dipole moment is consistent with the limited overlap of HOMO and LUMO orbitals and the intramolecular charge transfer nature of the lowest excited state from nitrogen to carbon. This spatial separation of the orbitals is responsible for the small singlet−triplet energy splitting and the charge transfer nature. The present study offers a method for probing the lowest excited states of conjugated flat chromophores with a magnetically allowed transition via supramolecular polymerization. We propose that such a photophysical understanding will pave the way for designing heptazine-based chiral materials for spin-controlled reactions such as water splitting.

ASSOCIATED CONTENT

Supporting Information

The Supporting Information is available free of charge at https://pubs.acs.org/doi/10.1021/jacs.4c02174.

The synthesis of *S*-**H**, NMR spectra for all compounds, FT-IR spectra, AFM images, additional experimental details, materials, and methods, including modeling and calculations, are shown in the Supporting Information (PDF)

AUTHOR INFORMATION

Corresponding Authors

Stefan Meskers − *Institute for Complex Molecular Systems and Molecular Materials and Nanosystems, Eindhoven University of Technology, Eindhoven 5600 MB, Netherlands;* orcid.org/0000-0001-9236-591X; Email: s.c.j.meskers@tue.nl

E. W. Meijer − *Institute for Complex Molecular Systems and Laboratory of Macromolecular and Organic Chemistry, Eindhoven University of Technology, Eindhoven 5600 MB, Netherlands; School of Chemistry and RNA Institute, UNSW, Sydney NSW 2052, Australia;* orcid.org/0000-0003-4126-7492; Email: e.w.meijer@tue.nl

Authors

Fan Xu − *Institute for Complex Molecular Systems and Laboratory of Macromolecular and Organic Chemistry, Eindhoven University of Technology, Eindhoven 5600 MB, Netherlands;* orcid.org/0000-0003-1615-1703

Hao Su − *Institute for Complex Molecular Systems and Laboratory of Macromolecular and Organic Chemistry, Eindhoven University of Technology, Eindhoven 5600 MB, Netherlands; College of Polymer Science and Engineering and State Key Laboratory of Polymer Materials Engineering, Sichuan University, Chengdu 610065, China;* orcid.org/0000-0003-0348-9828

Joost J. B. van der Tol − *Institute for Complex Molecular Systems and Laboratory of Macromolecular and Organic Chemistry, Eindhoven University of Technology, Eindhoven 5600 MB, Netherlands*

Stef A. H. Jansen − *Institute for Complex Molecular Systems and Laboratory of Macromolecular and Organic Chemistry, Eindhoven University of Technology, Eindhoven 5600 MB, Netherlands;* orcid.org/0000-0002-1505-8462

Youxin Fu − *Stratingh Institute for Chemistry, University of Groningen, Groningen 9747AG, Netherlands;* Present Address: Y.F.: Nanjing Forestry University, Nanjing 210 037, P.R. China

Giulia Lavarda − *Institute for Complex Molecular Systems and Laboratory of Macromolecular and Organic Chemistry, Eindhoven University of Technology, Eindhoven 5600 MB, Netherlands;* orcid.org/0000-0003-2171-008X

Ghislaine Vantomme − *Institute for Complex Molecular Systems and Laboratory of Macromolecular and Organic Chemistry, Eindhoven University of Technology, Eindhoven 5600 MB, Netherlands;* orcid.org/0000-0003-2036-8892

Complete contact information is available at: https://pubs.acs.org/10.1021/jacs.4c02174

Notes

The authors declare no competing financial interest.

ACKNOWLEDGMENTS

The authors acknowledge financial support from the Dutch Ministry of Education, Culture and Science (Gravity program 024.001.035) and European Research Council for funding (H2020-EU.1.1., SYNMAT-project, ID 788618). G.L. acknowledges a Marie Skłodowska-Curie Postdoctoral Individual Fellowship (101026072) for financial support. We thank Dr. Andreas Thomas Rösch and Nils Janssen for the synthesis and Prof. Wiktor Szymanski for providing the quantum yield measurement instrument.

REFERENCES

(1) Forrest, S. R. *Organic Electronics: Foundations to Applications*; Oxford University Press: USA, 2020.

(2) Mori, T. Chiroptical Properties of Symmetric Double, Triple, and Multiple Helicenes. *Chem. Rev.* **2021**, *121* (4), 2373−2412.

(3) Ghasemabadi, P. G.; Yao, T.; Bodwell, G. J. Cyclophanes Containing Large Polycyclic Aromatic Hydrocarbons. *Chem. Soc. Rev.* **2015**, *44* (18), 6494−6518.

(4) Kumar, S.; Tao, Y. T. Coronenes, Benzocoronenes and Beyond: Modern Aspects of Their Syntheses, Properties, and Applications. *Chem. An Asian J.* **2021**, *16* (6), 621−647.

(5) Segawa, Y.; Levine, D. R.; Itami, K. Topologically Unique Molecular Nanocarbons. *Acc. Chem. Res.* **2019**, *52* (10), 2760−2767.

(6) Yan, C.; Barlow, S.; Wang, Z.; Yan, H.; Jen, A. K. Y.; Marder, S. R.; Zhan, X. Non-Fullerene Acceptors for Organic Solar Cells. *Nat. Rev. Mater.* **2018**, *3*, 1−19.

(7) Wadsworth, A.; Moser, M.; Marks, A.; Little, M. S.; Gasparini, N.; Brabec, C. J.; Baran, D.; McCulloch, I. Critical Review of the Molecular Design Progress in Non-Fullerene Electron Acceptors towards Commercially Viable Organic Solar Cells. *Chem. Soc. Rev.* **2019**, *48* (6), 1596−1625.

(8) Audebert, P.; Kroke, E.; Posern, C.; Lee, S.-H. State of the Art in the Preparation and Properties of Molecular Monomeric *s*

-Heptazines: Syntheses, Characteristics, and Functional Applications. *Chem. Rev.* **2021**, *121* (4), 2515−2544.
(9) Li, J.; Nakagawa, T.; Macdonald, J.; Zhang, Q.; Nomura, H.; Miyazaki, H.; Adachi, C. Highly Efficient Organic Light-Emitting Diode Based on a Hidden Thermally Activated Delayed Fluorescence Channel in a Heptazine Derivative. *Adv. Mater.* **2013**, *25* (24), 3319−3323.
(10) Ehrmaier, J.; Rabe, E. J.; Pristash, S. R.; Corp, K. L.; Schlenker, C. W.; Sobolewski, A. L.; Domcke, W. Singlet−Triplet Inversion in Heptazine and in Polymeric Carbon Nitrides. *J. Phys. Chem. A* **2019**, *123* (38), 8099−8108.
(11) Aizawa, N.; Pu, Y.-J.; Harabuchi, Y.; Nihonyanagi, A.; Ibuka, R.; Inuzuka, H.; Dhara, B.; Koyama, Y.; Nakayama, K.-I.; Maeda, S.; Araoka, F.; Miyajima, D. Delayed Fluorescence from Inverted Singlet and Triplet Excited States. *Nature* **2022**, *609* (7927), 502−506.
(12) Zhang, G.; Lin, L.; Li, G.; Zhang, Y.; Savateev, A.; Zafeiratos, S.; Wang, X.; Antonietti, M. Ionothermal Synthesis of Triazine−Heptazine-Based Copolymers with Apparent Quantum Yields of 60% at 420 Nm for Solar Hydrogen Production from "Sea Water. *Angew. Chem., Int. Ed.* **2018**, *130* (30), 9516−9520.
(13) Ehrmaier, J.; Karsili, T. N. V.; Sobolewski, A. L.; Domcke, W. Mechanism of Photocatalytic Water Splitting with Graphitic Carbon Nitride: Photochemistry of the Heptazine-Water Complex. *J. Phys. Chem. A* **2017**, *121* (25), 4754−4764.
(14) Zhang, J.; Liang, X.; Zhang, C.; Lin, L.; Xing, W.; Yu, Z.; Zhang, G.; Wang, X. Improved Charge Separation in Poly(Heptazine-Triazine) Imides with Semi-Coherent Interfaces for Photocatalytic Hydrogen Evolution. *Angew. Chem., Int. Ed.* **2022**, *61*, 47.
(15) Cheng, H.; Lv, H.; Cheng, J.; Wang, L.; Wu, X.; Xu, H. Rational Design of Covalent Heptazine Frameworks with Spatially Separated Redox Centers for High-Efficiency Photocatalytic Hydrogen Peroxide Production. *Adv. Mater.* **2022**, *34* (7), 2107480.
(16) Berova, N.; Nakanishi, K.; Woody, R. W. *Circular Dichroism: Principles and Applications*; John Wiley & Sons, 2000.
(17) Meskers, S. C. J. Circular Polarization of Luminescence as a Tool To Study Molecular Dynamical Processes. *ChemPhotoChem.* **2022**, *6* (1), No. e202100154.
(18) Arrico, L.; Di Bari, L.; Zinna, F. Quantifying the Overall Efficiency of Circularly Polarized Emitters. *Chem. − A Eur. J.* **2021**, *27* (9), 2920−2934.
(19) Hasegawa, M.; Nojima, Y.; Mazaki, Y. Circularly Polarized Luminescence in Chiral Π-Conjugated Macrocycles. *ChemPhotoChem* **2021**, *5* (12), 1042−1058.
(20) Tian, X.; Shoyama, K.; Mahlmeister, B.; Brust, F.; Stolte, M.; Würthner, F. Naphthalimide-Annulated [n]Helicenes: Red Circularly Polarized Light Emitters. *J. Am. Chem. Soc.* **2023**, *145* (17), 9886−9894.
(21) Huo, G.-F.; Fukunaga, T. M.; Hou, X.; Han, Y.; Fan, W.; Wu, S.; Isobe, H.; Wu, J. Facile Synthesis and Chiral Resolution of Expanded Helicenes with up to 35 Cata-Fused Benzene Rings**. *Angew. Chem., Int. Ed.* **2023**, *62* (18), No. e202218090.
(22) Xu, Y.; Ni, Z.; Xiao, Y.; Chen, Z.; Wang, S.; Gai, L.; Zheng, Y.-X.; Shen, Z.; Lu, H.; Guo, Z. Helical *β*-Isoindigo-Based Chromophores with B−O−B Bridge: Facile Synthesis and Tunable Near-Infrared Circularly Polarized Luminescence. *Angew. Chem., Int. Ed.* **2023**, *62* (8), No. e202218023.
(23) Izquierdo-García, P.; Fernández-García, J. M.; Medina Rivero, S.; Šámal, M.; Rybáček, J.; Bednárová, L.; Ramírez-Barroso, S.; Ramírez, F. J.; Rodríguez, R.; Perles, J.; et al. Helical Bilayer Nanographenes: Impact of the Helicene Length on the Structural, Electrochemical, Photophysical, and Chiroptical Properties. *J. Am. Chem. Soc.* **2023**, *145* (21), 11599−11610.
(24) Li, J. K.; Chen, X. Y.; Guo, Y. L.; Wang, X. C.; Sue, A. C. H.; Cao, X. Y.; Wang, X. Y. B,N-Embedded Double Hetero[7]Helicenes with Strong Chiroptical Responses in the Visible Light Region. *J. Am. Chem. Soc.* **2021**, *143* (43), 17958−17963.
(25) Nakakuki, Y.; Hirose, T.; Sotome, H.; Miyasaka, H.; Matsuda, K. Hexa-Peri-Hexabenzo[7]Helicene: Homogeneously *π*-Extended Helicene as a Primary Substructure of Helically Twisted Chiral Graphenes. *J. Am. Chem. Soc.* **2018**, *140* (12), 4317−4326.
(26) Fukunaga, T. M.; Sawabe, C.; Matsuno, T.; Takeya, J.; Okamoto, T.; Isobe, H. Manipulations of Chiroptical Properties in Belt-Persistent Cycloarylenes via Desymmetrization with Heteroatom Doping. *Angew. Chem., Int. Ed.* **2021**, *60* (35), 19097−19101.
(27) Meng, D.; Liu, G.; Xiao, C.; Shi, Y.; Zhang, L.; Jiang, L.; Baldridge, K. K.; Li, Y.; Siegel, J. S.; Wang, Z. Corannurylene Pentapetalae. *J. Am. Chem. Soc.* **2019**, *141* (13), 5402−5408.
(28) Liu, B.; Böckmann, M.; Jiang, W.; Doltsinis, N. L.; Wang, Z. Perylene Diimide-Embedded Double [8]Helicenes. *J. Am. Chem. Soc* **2020**, *142* (15), 7092−7099.
(29) Liu, Y.; Ma, Z.; Wang, Z.; Jiang, W. Boosting Circularly Polarized Luminescence Performance by a Double *π*-Helix and Heteroannulation. *J. Am. Chem. Soc.* **2022**, *144* (25), 11397−11404.
(30) Kubo, H.; Hirose, T.; Nakashima, T.; Kawai, T.; Hasegawa, J.; Matsuda, K. Tuning Transition Electric and Magnetic Dipole Moments: [7]Helicenes Showing Intense Circularly Polarized Luminescence. *J. Phys. Chem. Lett.* **2021**, *12* (1), 686−695.
(31) Sakamaki, D.; Tanaka, S.; Tanaka, K.; Takino, M.; Gon, M.; Tanaka, K.; Hirose, T.; Hirobe, D.; Yamamoto, H. M.; Fujiwara, H. Double Heterohelicenes Composed of Benzo[b]- and Dibenzo[b,i]-Phenoxazine: A Comprehensive Comparison of Their Electronic and Chiroptical Properties. *J. Phys. Chem. Lett.* **2021**, *12* (38), 9283−9292.
(32) Mateos-Timoneda, M. A.; Crego-Calama, M.; Reinhoudt, D. N. Supramolecular Chirality of Self-Assembled Systems in Solution. *Chem. Soc. Rev.* **2004**, *33* (6), 363−372.
(33) Liu, M.; Zhang, L.; Wang, T. Supramolecular Chirality in Self-Assembled Systems. *Chem. Rev.* **2015**, *115* (15), 7304−7397.
(34) Kim, Y.-H; Zhai, Y.; Lu, H.; Pan, X.; Xiao, C.; Gaulding, E. A.; et al. Chiral-Induced Spin Selectivity Enables a Room-Temperature Spin Light-Emitting Diode. *Science* **2021**, *371*, 1129−1133.
(35) Lu, H.; Wang, J.; Xiao, C.; Pan, X.; Chen, X.; Brunecky, R.; Berry, J. J.; Zhu, K.; Beard, M. C.; Vardeny, Z. V. Spin-Dependent Charge Transport through 2D Chiral Hybrid Lead-Iodide Perovskites. *Sci. Adv.* **2019**, *5* (12), 1−8.
(36) Qian, Q.; Ren, H.; Zhou, J.; Wan, Z.; Zhou, J.; Yan, X.; Cai, J.; Wang, P.; Li, B.; Sofer, Z.; et al. Chiral Molecular Intercalation Superlattices. *Nature* **2022**, *606* (7916), 902−908.
(37) Kulkarni, C.; Mondal, A. K.; Das, T. K.; Grinbom, G.; Tassinari, F.; Mabesoone, M. F. J.; Meijer, E. W.; Naaman, R. Highly Efficient and Tunable Filtering of Electrons' Spin by Supramolecular Chirality of Nanofiber-Based Materials. *Adv. Mater.* **2020**, *32* (7), 1904965.
(38) Zhu, Q.; Danowski, W.; Mondal, A. K.; Tassinari, F.; Beek, C. L. F.; Heideman, G. H.; Santra, K.; Cohen, S. R.; Feringa, B. L.; Naaman, R. Multistate Switching of Spin Selectivity in Electron Transport through Light-Driven Molecular Motors. *Adv. Sci.* **2021**, *8* (18), 2101773.
(39) Brunsveld, L.; Folmer, B. J. B.; Meijer, E. W.; Sijbesma, R. P. Supramolecular Polymers. *Chem. Rev.* **2001**, *101* (12), 4071−4098.
(40) De Greef, T. F. A.; Smulders, M. M. J.; Wolffs, M.; Schenning, A. P. H. J.; Sijbesma, R. P.; Meijer, E. W. Supramolecular Polymerization. *Chem. Rev.* **2009**, *109* (11), 5687−5754.
(41) Ślęczkowski, M. L.; Mabesoone, M. F. J. J.; Ślęczkowski, P.; Palmans, A. R. A. A.; Meijer, E. W. Competition between Chiral Solvents and Chiral Monomers in the Helical Bias of Supramolecular Polymers. *Nat. Chem.* **2021**, *13* (2), 200−207.
(42) Palmans, A. R. A.; Meijer, E. W. Amplification of Chirality in Dynamic Supramolecular Aggregates. *Angew. Chem., Int. Ed.* **2007**, *46* (47), 8948−8968.
(43) Xu, F.; Crespi, S.; Pacella, G.; Fu, Y.; Stuart, M. C. A.; Zhang, Q.; Portale, G.; Feringa, B. L. Dynamic Control of a Multistate Chiral Supramolecular Polymer in Water. *J. Am. Chem. Soc.* **2022**, *144* (13), 6019−6027.
(44) Mabesoone, M. F. J.; Palmans, A. R. A.; Meijer, E. W. Solute-Solvent Interactions in Modern Physical Organic Chemistry: Supramolecular Polymers as a Muse. *J. Am. Chem. Soc.* **2020**, *142* (47), 19781−19798.

https://doi.org/10.1021/jacs.4c02174
J. Am. Chem. Soc. 2024, 146, 15843−15849

(45) Korevaar, P. A.; George, S. J.; Markvoort, A. J.; Smulders, M. M. J.; Hilbers, P. A. J.; Schenning, A. P. H. J.; De Greef, T. F. A.; Meijer, E. W. Pathway Complexity in Supramolecular Polymerization. *Nature* **2012**, *481* (7382), 492−496.
(46) Adelizzi, B.; Mabesoone, M. F. J.; Meng, X.; Aloi, A.; Zha, R. H.; Lutz, M.; Filot, I. A. W.; Palmans, A. R. A.; Meijer, E. W. Potential Enthalpic Energy of Water in Oils Exploited to Control Supramolecular Structure. *Nature* **2018**, *558* (7708), 100−103.
(47) Wehner, M.; Würthner, F. Supramolecular Polymerization through Kinetic Pathway Control and Living Chain Growth. *Nat. Rev. Chem.* **2020**, *4* (1), 38−53.
(48) Xu, F.; Crespi, S.; Pfeifer, L.; Stuart, M. C. A.; Feringa, B. L. Mechanistic Insight into Supramolecular Polymerization in Water Tunable by Molecular Geometry. *CCS Chem.* **2022**, *4* (7), 2212−2220.
(49) van der Tol, J. J. B.; Vantomme, G.; Meijer, E. W. Solvent-Induced Pathway Complexity of Supramolecular Polymerization Unveiled Using the Hansen Solubility Parameters. *J. Am. Chem. Soc.* **2023**, *145* (32), 17987−17994.
(50) Mabesoone, M. F. J.; Markvoort, A. J.; Banno, M.; Yamaguchi, T.; Helmich, F.; Naito, Y.; Yashima, E.; Palmans, A. R. A.; Meijer, E. W. Competing Interactions in Hierarchical Porphyrin Self-Assembly Introduce Robustness in Pathway Complexity. *J. Am. Chem. Soc.* **2018**, *140* (25), 7810−7819.
(51) Aida, T.; Meijer, E. W.; Stupp, S. I. Functional Supramolecular Polymers. *Science* **2012**, *335* (6070), 813−817.
(52) Hashim, P. K.; Bergueiro, J.; Meijer, E. W.; Aida, T. Supramolecular Polymerization: A Conceptual Expansion for Innovative Materials. *Prog. Polym. Sci.* **2020**, *105*, 101250.
(53) Xu, F.; Pfeifer, L.; Crespi, S.; Leung, F. K. C.; Stuart, M. C. A.; Wezenberg, S. J.; Feringa, B. L. From Photoinduced Supramolecular Polymerization to Responsive Organogels. *J. Am. Chem. Soc.* **2021**, *143* (15), 5990−5997.
(54) Dumele, O.; Chen, J.; Passarelli, J. V.; Stupp, S. I. Supramolecular Energy Materials. *Adv. Mater.* **2020**, *32* (17), 1−32.
(55) Xu, F.; Feringa, B. L. Photoresponsive Supramolecular Polymers: From Light-Controlled Small Molecules to Smart Materials. *Adv. Mater.* **2023**, *35* (10), 2204413.
(56) Yang, L.; Tan, X.; Wang, Z.; Zhang, X. Supramolecular Polymers: Historical Development, Preparation, Characterization, and Functions. *Chem. Rev.* **2015**, *115* (15), 7196−7239.
(57) Domcke, W.; Sobolewski, A. L.; Schlenker, C. W. Photooxidation of Water with Heptazine-Based Molecular Photocatalysts: Insights from Spectroscopy and Computational Chemistry. *J. Chem. Phys.* **2020**, *153* (10), 100902.
(58) Emeis, C. A.; Oosterhoff, L. J. The N-Π* Absorption and Emission of Optically Active Trans-β -Hydrindanone and Trans-β -Thiohydrindanone. *J. Chem. Phys.* **1971**, *54* (11), 4809−4819.

https://doi.org/10.1021/jacs.4c02174
J. Am. Chem. Soc. 2024, 146, 15843−15849